

Self-tuned Quantum Criticality and Non-Fermi-liquid in a Yukawa-SYK Model: a Quantum Monte Carlo Study

Gaopei Pan,^{1,2} Yuxuan Wang,^{3,*} and Zi Yang Meng^{4,1,5,†}

¹*Beijing National Laboratory for Condensed Matter Physics and Institute of Physics, Chinese Academy of Sciences, Beijing 100190, China*

²*School of Physical Sciences, University of Chinese Academy of Sciences, Beijing 100190, China*

³*Department of Physics, University of Florida, Gainesville, FL 32601*

⁴*Department of Physics and HKU-UCAS Joint Institute of Theoretical and Computational Physics, The University of Hong Kong, Pokfulam Road, Hong Kong, China*

⁵*Songshan Lake Materials Laboratory, Dongguan, Guangdong 523808, China*

(Dated: December 21, 2024)

Non-Fermi liquids (nFL) are a class of strongly interacting gapless fermionic systems without long-lived quasiparticle excitations. An important type of models for nFL features itinerant fermions coupled to soft bosonic fluctuations near a quantum-critical point (QCP), widely believed to be related to the essential physics of many unconventional superconductors. However numerically the direct observation of a canonical nFL behavior, characterized by a power-law form in the Green's function, has been elusive. Sachdev-Ye-Kitaev (SYK) models offer a new route to construct models of nFL's with a solvable large- N limit. Here we consider an SYK-like model with random Yukawa interaction (Yukawa-SYK model) between critical bosons and fermions, and show it can be constructed without minus-sign problem and hence solved exactly via large-scale quantum Monte Carlo simulation beyond the large- N limit accessible to analytical approaches. At large- N , this model features “self-tuned quantum criticality”, i.e., the system is critical independent of the bosonic bare mass. We put these results to test at finite N and show clear evidence of such exotic quantum-critical nFL. We report signatures of pairing fluctuations at lower temperatures. These results shed light on the theoretical understanding of Planckian metals and high temperature superconductors.

I. INTRODUCTION

The non-Fermi liquid (nFL) is a state of gapless fermionic matter that does not have long-lived quasiparticles due to its strongly interacting nature [1, 2]. It is widely believed to be the microscopic origin of the “strange metal” state observed in a broad range of materials, such as Cu-base [3] and Fe-based [4, 5] high-temperature superconductors, heavy-fermion compounds [6, 7], and recently in twisted bilayer graphene [8]. Importantly, the understanding of the unconventional superconducting phase in these systems naturally hinges on the understanding of the nFL “normal state”. Moreover, recently from the studies of the Sachdev-Ye-Kitaev (SYK) models [9–12], it has been realized that nFLs host a hidden connection with holographic quantum matters that saturate the upper bound for quantum chaos due to its short equilibration time, opening an entirely new avenue in understanding the behavior of nFLs [13].

In a general context, nFL behavior often occur via electron interactions mediated by gapless bosonic modes [14–25] that render the electrons incoherent. Such gapless bosons typically arise in the vicinity of a quantum-critical point (QCP) or in gauge theories. Despite the simple setup, the analytical solution to these models remains challenging due to the lack of a natural small control parameter. Advancement has been made via modifying the

model to a large N limit with N the number of fermion flavors and a leap of faith that the same physics holds down to $N = O(1)$, while these large- N approaches face important subtleties in two spatial dimensions [26].

Along a separate path, there has been great progress in the numerical front in recent years, in particular in designer Hamiltonian of critical bosons Yukawa-coupled to Fermi surfaces [25, 27, 28]. Recent results in minus-sign-problem-free quantum Monte Carlo (QMC) simulations [21–25, 28] have shown strong evidence of nFL states in a range of such boson-fermion models upon tuning the boson mass to criticality. Such a new pathway towards large-scale unbiased simulations of fermionic QCPs are now available and the nematic [29], ferromagnetic [21], antiferromagnetic [22, 23, 30–32] and matter field coupled to gauge field [24, 33] QCPs have been explored (see Ref. [25] for a recent review). It is now possible to obtain accurate and reliable information about the scaling behaviors in the close vicinity of these QCPs, to test and improve our theoretical knowledge about these challenging problems.

To reveal nFL physics in numerics, this class of models requires tuning the mass of the boson to a critical value, while away from the QCP the system restores Fermi liquid behavior. However, to date there has not been direct evidence of nFL behavior in the Green's functions at the quantum critical point, characterized by a power-law form in the fermionic self-energy. Instead, QMC simulations around the Ising-nematic [29], Ising-ferromagnetic [21] and Ising-antiferromagnetic [23] critical points have reported either small constant or slowly

* yuxuan.wang@ufl.edu

† zymeng@hku.hk

increasing low-frequency self-energies, likely due to pairing fluctuations or finite size effects [34]. Intensive studies to account for such puzzling observations in this class of models are still ongoing.

Recently a class of SYK-like models featuring random Yukawa interactions between bosons and fermions has been put forward to address the nFL pairing problem [35–37]. Similar to the SYK models, these “Yukawa-SYK model” strip space from the degrees of freedom and in a large- N limit become analytically solvable. Just like the SYK model, the Yukawa-SYK models have been shown to be maximally chaotic [38] and thus likely to admit a holographic dual. Compared with the SYK models that only involve interacting fermions, the inclusion of a dynamical bosonic degree of freedom in the Yukawa-SYK makes it ideal to model itinerant fermionic systems near a QCP. Unlike finite dimensional models, within large- N approximation these models have been shown to be “self-tuned” to quantum criticality, i.e., the system becomes critical due to the strong mutual feedback between the bosonic and fermionic sectors, independent of the bosonic bare mass. In addition, the pairing behavior at large- N has been analytically studied [35–37]. Depending on details of the Yukawa coupling, these models either shows exotic pairing of nFL, or a nFL phase that is stable to pairing down to $T = 0$.

However, these remarkable analytical results are only accessible at $N \rightarrow \infty$ and become uncontrolled at finite N . Unbiased numeric calculation, similar in the spirit of the aforementioned critical bosons Yukawa-coupled to Fermi surfaces systems [21–25, 27–30, 33], are in great need to provide concrete results. In this work, we address such a timely issue by showing that at finite N the Yukawa-SYK model can be exactly solved by QMC simulations, thanks to the dynamical bosonic degree of freedom. A simple extension of the original model, introducing an antiunitary time-reversal symmetry, eliminates the minus-sign problem in the determinantal quantum Monte Carlo framework without altering the essential physics. As an important feature for SYK-like models, the Yukawa-SYK model has an emergent reparametrization [11, 12] symmetry that allows for, at large M, N , an analytical universal expression of the Green’s functions in the long-time limit at finite temperatures. Quite nicely, this means that one does not need to go to very low temperatures to search for analytically predicted nFL behavior, enhancing the efficiency of QMC methods.

The main discovery of this paper is thus as follows. Employing large-scale QMC simulations, we show that even at finite N and M , this model indeed exhibits self-

tuned quantum-critical and nFL behaviors. We verify this by using the conformal symmetry of the Schwinger-Dyson equations to obtain the analytical nFL behavior at finite temperatures at $N, M \rightarrow \infty$, and comparing it with our numerical results. Remarkably we confirm that the quantum-critical and nFL behavior is robust against tuning the bare mass of the bosons, in sharp contrast to prior QMC and analytical results for finite-dimensional models. We show that already at finite $N = M = 6$, and inverse temperature $\beta = 8$ and 12, the anomalous dimensions of the fermions and bosons exhibit an excellent agreement with the analytical results. By going to low temperatures at $M = 2$ and $N = 2$, we further show that pairing fluctuations become strong and alter the fermionic self-energy from the nFL scaling behavior at higher temperatures. However, such a deviation from nFL sets in at temperatures much lower than the prediction of the mean-field theory at $M \rightarrow \infty, N \rightarrow \infty$. Nevertheless this result provides a foundation for a more complete understanding of pairing emerging from nFL “parent state”.

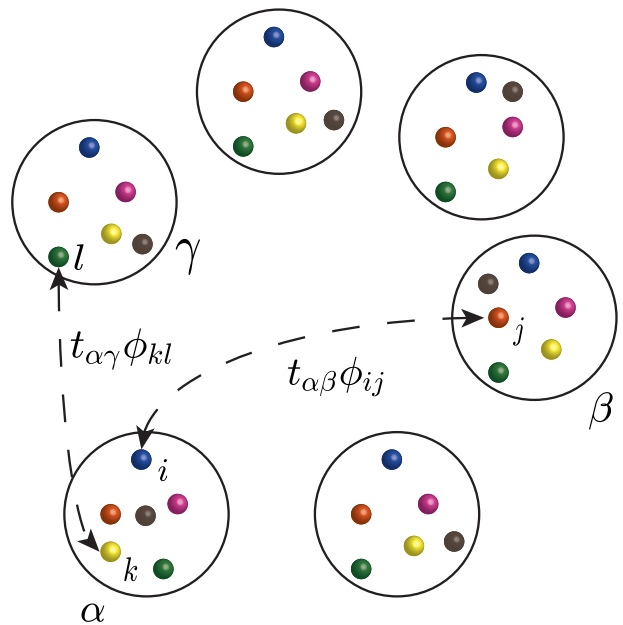


FIG. 1. Yukawa-SYK model. There are $\alpha, \beta = 1, \dots, M$ quantum dots, each dot acquires $i, j = 1, \dots, N$ flavors. Fermions are Yukawa coupled via the random hopping $t_{\alpha\beta}$ and anti-symmetric bosonic field ϕ_{ij} as $t_{\alpha\beta}\phi_{ij}c_{i\alpha m}^\dagger\sigma_{m,n}^z c_{j\beta n}$.

II. THE MODEL

The model studied here is a modification from that in Ref. [35] and it reads

$$H = \sum_{i,j=1}^N \sum_{\alpha,\beta=1}^M \sum_{\uparrow,\downarrow} \left(\frac{i}{\sqrt{MN}} t_{\alpha\beta} \phi_{ij} c_{i\alpha m}^\dagger \sigma_{m,n}^z c_{j\beta n} \right) + \sum_{i,j=1}^N \left(\frac{1}{2} \pi_{ij}^2 + \frac{M}{N} \frac{m_0^2}{2} \phi_{ij}^2 \right), \quad (1)$$

where the random coupling between fermion and boson is realized as $\langle t_{\alpha\beta} \rangle = 0$, $\langle t_{\alpha\beta} t_{\gamma\delta} \rangle = (\delta_{\alpha\gamma} \delta_{\beta\delta} + \delta_{\alpha\delta} \delta_{\beta\gamma}) \omega_0^3$, for the sake of simplicity we set $\omega_0 = 1$ as the energy unit throughout the paper, and the temperature scale is then $T \equiv \omega_0/\beta$. π_{ij} is the canonical momentum of ϕ_{ij} . Hermiticity of the first term requires $\phi_{ij} = -\phi_{ji}$. As schematically depicted in Fig. 1, here (i, j) are flavor indices and (α, β) are quantum dot indices. σ^z is the Pauli matrix in the fermion spin space for each flavor. In the $N \rightarrow \infty, M \rightarrow \infty$ limit, the ground state of the system can be analytically solved [35]. However, for finite N, M , the analytical results are no longer reliable. Fortunately, due to a time-reversal symmetry $\mathcal{T} = i\sigma_y \mathcal{K}$ in our designer Hamiltonian in Eq. (1) there is no minus-sign problem (the proof of this step is given in Sec. III C.), and one can perform QMC simulations.

A. Normal-state results at $N, M \rightarrow \infty$

Before demonstrating our QMC results for the Yukawa-SYK model, we first outline analytical expectations at the $N, M \rightarrow \infty$ limit in this section.

At the low-energy limit, one can neglect the bare frequency dependence of the fermionic and bosonic Green's functions,

$$\begin{aligned} \Sigma(\tau, \bar{\tau}) &= \omega_0^3 G_f(\tau, \bar{\tau}) G_b(\tau, \bar{\tau}) \\ \Pi(\tau, \bar{\tau}) &= 4\omega_0^3 \frac{M}{N} [G_f(\tau, \bar{\tau})]^2 \\ \delta(\tau - \bar{\tau}) &= \int d\tilde{\tau} G_b(\tau, \tilde{\tau}) \left[\frac{M}{N} m_0^2 \delta(\tilde{\tau} - \bar{\tau}) + \Pi(\tilde{\tau}, \bar{\tau}) \right] \\ \delta(\tau - \bar{\tau}) &= - \int d\tilde{\tau} G_f(\tau, \tilde{\tau}) \Sigma(\tilde{\tau}, \bar{\tau}), \end{aligned} \quad (2)$$

where $\tau, \bar{\tau}, \tilde{\tau}$ are imaginary times, Σ, Π are fermionic and bosonic self-energies, and G_f, G_b are fermionic and bosonic Green's functions.

Eq. (2) has been solved in the (Matsubara) frequency domain in Ref. [35] (see also Ref. [36]). It was found that for $m_0 \sim \omega_0$ and $\omega, \Omega \ll \omega_0$ the self-energies are given by

$$\begin{aligned} \Sigma(\omega) &= -G_f(\omega)^{-1} = ic \operatorname{sgn}(\omega) |\omega|^x \omega_0^{1-x}, \\ \Pi(\Omega) &= G_b(\Omega)^{-1} = -\frac{M}{N} m_0^2 + c^{-2} \alpha(x) |\Omega|^{1-2x} \omega_0^{1+2x}, \end{aligned} \quad (3)$$

where c is an $O(1)$ constant, and $0 < x < 1/2$ is determined by

$$\frac{4M}{N} = \frac{1/x - 2}{1 + \sec(\pi x)} \quad (4)$$

and

$$\alpha(x) = -\frac{\Gamma^2(-x)}{4\pi\Gamma(-2x)}. \quad (5)$$

Compared to the results in Ref. [35], Eq. (4) is different by a factor of 2 because the addition of the spin degree of freedom $m, n = \uparrow / \downarrow$ in the Hamiltonian in Eq. (1). In particular, at $M = N$, one finds $x \approx 0.098$.

From Eq. (2) we have

$$\frac{M}{N} m_0^2 - \Pi(\Omega = 0) = 0, \quad (6)$$

which means the boson is critical. This was shown in Refs. [35, 36] to be true for an *arbitrary* m_0^2 . No matter what the bosonic bare mass is, the system renormalizes it to zero via interaction effects. For this reason we dub this phenomenon ‘‘self-tuned quantum criticality’’, which is not present in any finite dimensional models such as those of critical bosons coupled to Fermi surface systems [14–25, 28–31, 33] discussed in Sec. I.

In the time domain, by a Fourier transform we obtain [39]

$$\begin{aligned} \Pi(\tau, \bar{\tau}) &\propto |\tau - \bar{\tau}|^{-(2-2x)}, \\ G_b(\tau, \bar{\tau}) &\propto |\tau - \bar{\tau}|^{-2x} \\ \Sigma(\tau, \bar{\tau}) &\propto |\tau - \bar{\tau}|^{-(1+x)} \operatorname{sgn}(\tau - \bar{\tau}), \\ G_f(\tau, \bar{\tau}) &\propto |\tau - \bar{\tau}|^{x-1} \operatorname{sgn}(\tau - \bar{\tau}) \end{aligned} \quad (7)$$

At finite temperatures, typically the Green's functions do not have a universal expression. However, here in our case one can make use of an approximate reparametrization symmetry of Eq. (2) to obtain an analytical solution, much like the SYK model. In the long time limit of Eq. (2), (neglecting the short-time $m_0^2 \delta(\tilde{\tau} - \bar{\tau})$ term), $\Sigma(\tau, \bar{\tau})$ and $\Pi(\tau, \bar{\tau})$ has an approximate reparametrization symmetry — their equations are invariant under

$$\begin{aligned} \Sigma(\tau, \bar{\tau}) &\rightarrow f'(\tau)^{\frac{1+x}{2}} f'(\bar{\tau})^{\frac{1+x}{2}} \Sigma(f(\tau), f(\bar{\tau})) \\ \Pi(\tau, \bar{\tau}) &\rightarrow f'(\tau)^{1-x} f'(\bar{\tau})^{1-x} \Pi(f(\tau), f(\bar{\tau})) \\ G_f(\tau, \bar{\tau}) &\rightarrow f'(\tau)^{\frac{1-x}{2}} f'(\bar{\tau})^{\frac{1-x}{2}} G_f(f(\tau), f(\bar{\tau})) \\ G_b(\tau, \bar{\tau}) &\rightarrow f'(\tau)^x f'(\bar{\tau})^x G_b(f(\tau), f(\bar{\tau})) \end{aligned} \quad (8)$$

At a finite temperature $T = 1/\beta$, one would accordingly get for the fermionic and bosonic Green's functions through the reparametrization $f(\tau) = \tan(\pi\tau/\beta)$, and we have

$$\begin{aligned} G_f(\tau, 0) &\propto \left(\frac{\pi}{\beta \sin(\pi\tau/\beta)} \right)^{1-x} \\ G_b(\tau, 0) &\propto \left(\frac{\pi}{\beta \sin(\pi\tau/\beta)} \right)^{2x}. \end{aligned} \quad (9)$$

The product of the bosonic Green's function with the square of fermionic Green's function, enjoys an universal behavior with integer power

$$G_b(\tau, 0)G_f(\tau, 0)^2 \propto \left(\frac{\pi}{\beta \sin(\pi\tau/\beta)} \right)^2. \quad (10)$$

These results can be directly compared with the QMC data.

B. Pairing at $N, M \rightarrow \infty$: Mean field theory

The leading pairing instability mediated by the critical boson mode is toward a spin-singlet, intra-dot, and intra-flavor channel:

$$\Delta \sim \sum_{i,\alpha} \langle c_{i\alpha\uparrow}^\dagger c_{i\alpha\downarrow}^\dagger \rangle. \quad (11)$$

Within mean-field theory, the pairing behavior is described by the Eliashberg equation

$$\Delta(\omega) = \omega_0^3 \int \frac{d\Omega}{2\pi} G_b(\Omega) |G_f(\omega + \Omega)|^2 \Delta(\omega + \Omega), \quad (12)$$

where the $1/MN$ factor given by the two Yukawa interaction vertices has been canceled by the summation of the site and flavor indices of the internal fermions. Plugging in the analytical results at $T = 0$ in Eq. (2), we have

$$\Delta(\omega) = \frac{2}{\alpha(x)} \int_{\Delta}^{\omega_0} \frac{d\omega'}{2\pi} \frac{\Delta(\omega')}{|\omega - \omega'|^{1-2x} |\omega'|^{2x}}. \quad (13)$$

where Δ is the order of magnitude of the frequency-dependent gap $\Delta(\omega)$ that serves as an infrared cutoff of the Green's functions, and $\omega_0 \sim m_0$ is an ultraviolet cutoff scale for the low-energy quantum-critical nFL behavior. The value of Δ can also be regarded as the scale of the critical temperature T_c below which pairing sets in.

Notice that compared with the pairing problem in the spinless version of the problem in Ref. [35], where spin-singlet pairing channel is absent, the effective pairing interaction is enhanced by a factor of M . Since there is no small parameter in this pairing equation Eq. (13), one cannot obtain an analytical result for Δ or the critical temperature T_c , other than the conclusion $\Delta \sim T_c = O(\omega_0)$. To obtain the pairing behavior of this present model, one needs to rely on numerical results.

III. DQMC METHODOLOGY

The model described in Eq. (1) can be solved under the framework of determinant quantum Monte Carlo (DQMC) [25, 40–43]. DQMC is the method of choice to study the interaction electron systems and has been used extensively in the past few decades in the addressing the problem such as Hubbard [42], $t - J$ [44] and Kondo lattice [45] models, and lately some great progress have been made in extending the DQMC scheme to interacting topological state of matter [46, 47], duality and QCP beyond Landau-Ginzburg-Wilson paradigm [48, 49], and more relevant to this work, the designer Hamiltonians of critical boson coupled to fermions via Yukawa interactions [21–23, 25, 27, 28, 30–32, 50]. In this session, we will elucidate the DQMC setting for model in Eq. (1) in detail.

First, the partition function reads

$$\begin{aligned} Z &= \text{Tr} \left\{ e^{-\beta \hat{H}} \right\} \\ &= \text{Tr} \left\{ \left(e^{-\Delta\tau \hat{H}} \right)^{L_\tau} \right\} \\ &= \int \left(\prod_{ij} d\phi_{ij} \right) \text{Tr}_{\mathbf{F}} \langle \phi_{11} \cdots \phi_{NN} | \left(e^{-\Delta\tau \hat{H}} \right)^{L_\tau} | \phi_{11} \cdots \phi_{NN} \rangle \end{aligned} \quad (14)$$

where we divide the imaginary time axis into L_τ slices, $\beta = L_\tau \times \Delta\tau$. Let the bosonic configuration at each time slice, $\vec{\Phi}_l = (\phi_{11,l}, \phi_{12,l}, \cdots, \phi_{N(N-1),l}, \phi_{NN,l})$, serves as the complete basis of imaginary time propagation in the path-integral, then

$$\begin{aligned} Z &= \int \left(\prod_{l=1}^{L_\tau} d\vec{\Phi}_l \right) \\ &\text{Tr}_{\mathbf{F}} \langle \vec{\Phi}_1 | e^{-\Delta\tau \hat{H}} | \vec{\Phi}_{L_\tau} \rangle \langle \vec{\Phi}_{L_\tau} | e^{-\Delta\tau \hat{H}} | \vec{\Phi}_{L_\tau-1} \rangle \cdots \\ &\cdots \langle \vec{\Phi}_2 | e^{-\Delta\tau \hat{H}} | \vec{\Phi}_1 \rangle. \end{aligned} \quad (15)$$

With the help of Suzuki's Trotter decomposition of the Hamiltonian in Eq. (1), one has

$$e^{-\Delta\tau \hat{H}} \approx e^{-\Delta\tau \hat{H}_{fb}} e^{-\Delta\tau \hat{H}_b} \quad (16)$$

where

$$H_{fb} = \sum_{i,j}^N \sum_{\alpha,\beta}^M \sum_{m,n}^{\uparrow\downarrow} \left(\frac{i}{\sqrt{MN}} t_{\alpha\beta} \phi_{ij} c_{i\alpha m}^\dagger \sigma_{m,n}^z c_{j\beta n} - \mu c_{i\alpha m}^\dagger c_{i\alpha m} \right) \quad (17)$$

$$H_b = \sum_{i,j=1}^N \left(\frac{1}{2} \pi_{ij}^2 + \frac{M}{N} \frac{m_0^2}{2} \phi_{ij}^2 \right), \quad (18)$$

are the fermion-boson coupled term and the bosonic term, respectively.

A. Bosonic Part

Since we use the space-time arrangement of the bosons $\{\vec{\Phi}_l\}$ to span the configuration space, we need to first express the canonical momentum π_{ij} in Eq. (18) in this configuration space. To this end, we first use the coherent state path integral

$$|\phi_{ij}\rangle = \frac{1}{\sqrt{2\pi}} \int d\pi_{ij} e^{-i\pi_{ij}\phi_{ij}} |\pi_{ij}\rangle \quad (19)$$

$$Z = \int \prod_{l=1}^{L_\tau} d\vec{\Phi}_l \underbrace{C^{L_\tau} \left(\prod_{l=1}^{L_\tau} \prod_{i,j=1}^N e^{-\Delta\tau \frac{M}{N} \frac{m_0^2}{2} \phi_{ij,l}^2} \right)}_{\mathcal{W}_b} \left(\prod_{\langle l,l' \rangle} \prod_{i,j=1}^N e^{-\frac{(\phi_{ij,l} - \phi_{ij,l'})^2}{2\Delta\tau}} \right) \underbrace{\text{Tr}_{\mathbf{F}} \left\{ e^{-\Delta\tau \hat{H}_{fb}(\vec{\Phi}_{L_\tau})} \dots e^{-\Delta\tau \hat{H}_{fb}(\vec{\Phi}_1)} \right\}}_{\mathcal{W}_{fb}} \quad (21)$$

where the first $(\)$ in \mathcal{W}_b contains the spatial boson interaction and the second $(\)$ in \mathcal{W}_b contains the temporal boson interaction with $\langle l, l' \rangle$ stands for the nearest-neighbor interaction in imaginary time direction, and the $\text{Tr}_{\mathbf{F}}$ in \mathcal{W}_{fb} is the fermion trace we will deal with in Sec. III B. It is now clear that the Monte Carlo sampling is performed in the bosonic field $\{\vec{\Phi}\}$ space of dimension $N \times N \times L_\tau$ or $MN \times MN \times L_\tau$ if one consider the random hopping $t_{\alpha\beta}$ in H_{fb} , the configurational weight is comprised of the bosonic part \mathcal{W}_b and the fermion determinant \mathcal{W}_{fb} .

B. Fermion determinant

For a specific bosonic configuration, the fermion determinant is of quadratic form and can be evaluated as that of the free system, following the standard expression

$$\text{Tr}_{\mathbf{F}} \left\{ e^{-\sum_{i,j} \hat{c}_i^\dagger A_{i,j} \hat{c}_j} e^{-\sum_{i,j} \hat{c}_i^\dagger B_{i,j} \hat{c}_j} \right\} = \text{Det} (\mathbf{I} + e^{-\mathbf{A}} e^{-\mathbf{B}}). \quad (22)$$

$$Z = \int \left(\prod_{l=1}^{L_\tau} d\vec{\Phi}_l \right) \underbrace{C^{L_\tau} \left(\prod_{l=1}^{L_\tau} \prod_{i,j=1}^N e^{-\Delta\tau \frac{M}{N} \frac{m_0^2}{2} \phi_{ij,l}^2} \right)}_{\mathcal{W}_b} \left(\prod_{\langle l,l' \rangle} \prod_{i,j=1}^N e^{-\frac{(\phi_{ij,l} - \phi_{ij,l'})^2}{2\Delta\tau}} \right) \underbrace{\text{Det}[\mathbf{1} + B(L_\tau \Delta\tau, (L_\tau - 1) \Delta\tau) \dots B(\Delta\tau, 0)]}_{\mathcal{W}_{fb}} \quad (25)$$

This is the partition function describing the SYK-Yukawa model in Eq. (1) and we can now simulate it in DQMC.

C. Free from sign problem

As aforementioned, the partition function in Eq. (25) is free from the minus-sign problem in the protection of

then the momentum term in the partition function can be expressed as

$$\begin{aligned} \langle \phi' | e^{-\frac{1}{2}\Delta\tau \hat{\pi}^2} | \phi \rangle &= \frac{1}{2\pi} \int d\pi e^{i\pi(\phi' - \phi) - \frac{1}{2}\pi^2 \Delta\tau} \\ &\simeq C e^{-\frac{(\phi' - \phi)^2}{2\Delta\tau}} \end{aligned} \quad (20)$$

where C is a constant, and l and l' are two consecutive time slices along the imaginary time axis, and the partition function then becomes

For the imaginary time propagation in the fermion trace in Eq. (21), we define

$$B(l_2 \Delta\tau, l_1 \Delta\tau) = \prod_{l=l_1+1}^{l_2} e^{-\Delta\tau V(\vec{\Phi}_l)} \quad (23)$$

where

$$V(\vec{\Phi}_l) = \frac{i}{\sqrt{MN}} \sigma_{2 \times 2}^z \otimes (t_{\alpha\beta})_{M \times M} \otimes (\phi_{ij,l})_{N \times N}. \quad (24)$$

It is interesting to note that in the conventional Hubbard-type model setting, there also exists a fermion hopping matrix on the exponential form, but since here we only have fermion Yukawa coupled with the bosonic field, that the hopping matrix is reduced to identical matrix, and the interaction matrix $V(\vec{\Phi}_l)$, which depends on the space-time configuration of the bosonic field $\{\vec{\Phi}_l\}$, contains both the randomness in hopping matrix $\sigma_{2 \times 2}^z \otimes (t_{\alpha,\beta})_{M \times M}$ and the bosonic fluctuation matrix $(\phi_{ij,l})_{N \times N}$. Such that after tracing out the fermion operators $c_{i\alpha m}^\dagger$ and $c_{j\beta n}$, the resulting fermion determinant is the determinant of matrices with size $MN \times MN$ and block diagonal in the fermion spin space of σ^z .

With these notations prepared, finally the partition function in Eq. (21) can now be written as

a time-reversal symmetry [51], i.e., the Hamiltonian is

invariant under such a symmetry operation, this can be easily demonstrated as follows.

First, we note

$$H_{fb} = \sum_{i,j=1}^N \sum_{\alpha,\beta=1}^M \frac{i}{\sqrt{MN}} t_{\alpha\beta} \phi_{ij} c_{i\alpha\uparrow}^\dagger c_{j\beta\uparrow} - \mu c_{i\alpha\uparrow}^\dagger c_{i\alpha\uparrow} - \frac{i}{\sqrt{MN}} t_{\alpha\beta} \phi_{ij} c_{i\alpha\downarrow}^\dagger c_{j\beta\downarrow} - \mu c_{i\alpha\downarrow}^\dagger c_{i\alpha\downarrow} \quad (26)$$

and time-reversal symmetry operator is $\mathcal{T} = i\sigma_y \mathcal{K}$. Its operation works as $\mathcal{T} c_m \mathcal{T}^{-1} = U_{nm} c_m$, $\mathcal{T} c_m^\dagger \mathcal{T}^{-1} = U_{nm}^* c_m^\dagger$, $\mathcal{T} i \mathcal{T}^{-1} = -i$, where $m, n = \uparrow / \downarrow$, $U = i\sigma_y$, then

$$\begin{aligned} \mathcal{T} H_{fb} \mathcal{T}^{-1} &= \sum_{i,j=1}^N \sum_{\alpha,\beta=1}^M -\frac{i}{\sqrt{MN}} t_{\alpha\beta} \phi_{ij} c_{i\alpha\downarrow}^\dagger c_{j\beta\downarrow} - \mu c_{i\alpha\downarrow}^\dagger c_{i\alpha\downarrow} \\ &\quad + \frac{i}{\sqrt{MN}} t_{\alpha\beta} \phi_{ij} c_{i\alpha\uparrow}^\dagger c_{j\beta\uparrow} - \mu c_{i\alpha\uparrow}^\dagger c_{i\alpha\uparrow} \\ &= H_{fb}, \end{aligned} \quad (27)$$

therefore H_{fb} is invariant under \mathcal{T} .

Next, notice that $V(\vec{\Phi}_l)$ is block diagonal in the space of $m, n = \uparrow, \downarrow$, then the fermion determinant can be written as

$$\begin{aligned} \text{Det}[\mathbf{1} + B(\beta, 0)] &= \text{Det}[\mathbf{1} + B^\uparrow(\beta, 0)] \text{Det}[\mathbf{1} + B^\downarrow(\beta, 0)] \\ &= \text{Det}[\mathbf{1} + B^\uparrow(\beta, 0)] \text{Det}[\mathcal{T}(\mathbf{1} + B^\downarrow(\beta, 0))\mathcal{T}^{-1}]^* \\ &= \text{Det}[\mathbf{1} + B^\uparrow(\beta, 0)] \text{Det}[\mathbf{1} + B^\uparrow(\beta, 0)]^* \\ &= |\text{Det}[\mathbf{1} + B^\uparrow(\beta, 0)]|^2 \end{aligned} \quad (28)$$

and it is positive definite. Also note that the boson weight \mathcal{W}_b is positive definite as the $\{\vec{\Phi}\}$ is the eigenstate of the H_b in the space-time. So the entire configurational weight is positive definite and there is no sign-problem for the simulation.

D. Update and measurement

Another important ingredient in any Monte Carlo simulation is the update scheme between configurations, here since the bosonic fields are continuous variables, we have to adapt to local update with Metropolis-type acceptance rate.

The ensemble average of physical observable can be expressed as:

$$\langle \hat{O} \rangle = \frac{\text{Tr} \left\{ e^{-\beta \hat{H}} \hat{O} \right\}}{\text{Tr} \left\{ e^{-\beta \hat{H}} \right\}} = \int \left(\prod_{l=1}^{L_\tau} d\vec{\Phi}_l \right) \mathcal{P}_C \langle \hat{O} \rangle_C + O(\Delta\tau^2) \quad (29)$$

where $\Delta\tau^2$ systematical error comes from the Trotter decomposition and the weight and expectation value for

each bosonic field configuration \mathcal{C} are

$$\mathcal{P}_C = \frac{\mathcal{W}_C^{fb} \text{Det}[\mathbf{1} + B_C(\beta, 0)]}{\int \left(\prod_{l=1}^{L_\tau} d\vec{\Phi}_l \right) \mathcal{W}_C^{fb} \text{Det}[\mathbf{1} + B_C(\beta, 0)]} \quad (30)$$

$$\langle \hat{O} \rangle_C = \frac{\text{Tr} \{ \hat{U}_C(\beta, \tau) \hat{O} \hat{U}_C(\tau, 0) \}}{\text{Tr} \{ \hat{U}_C(\beta, 0) \}}, \quad (31)$$

where

$$\hat{U}(l_2 \Delta\tau, l_1 \Delta\tau) = \prod_{l=l_1+1}^{l_2} e^{-\Delta\tau \hat{\epsilon}^\dagger V(\vec{\Phi}_l) \hat{\epsilon}} \quad (32)$$

here $\hat{\epsilon}$ has $2 \times M \times N$ components, so does the dimension of the matrix V . Once tracing out the quadratic fermions $\hat{\epsilon}$ in Eq. (32), one arrives at the $B(l_2 \Delta\tau, l_1 \Delta\tau)$ matrix in Eq. (23), and the evaluation of fermion determinant follows from there down to Eq. (25). The detailed derivation of physical observables, exemplified by the equal time and imaginary time displaced fermionic Green's functions, are given in Appendix A.

Moreover, since the coupling matrix $t_{\alpha\beta}$ in H_{fb} is subject to randomness, the aforementioned Monte Carlo sample is performed for each disorder realization. Therefore, besides the Monte Carlo average over a fixed disorder configuration, the final physical observables such as the fermion and boson Green's functions are the disordered averaged quantities.

IV. NUMERICAL RESULTS

In this section, we demonstrate the two key numerical discoveries in this paper, (i) the nFL and self-tuned quantum criticality at finite values of (M, N) , and (ii) the signature of fluctuating unconventional pairing originating from nFL.

A. nFL and self-tuned quantum criticality

In Fig. 2 we demonstrate the fermion and boson Green's functions obtained in QMC simulation indeed are consistent with the $N, M \rightarrow \infty$ results of Eq. (9) and (10). We focus on the bosonic and fermionic Green's functions, G_b and G_f , obtained at $M = N = 6$, $m_0 = \omega_0 = 1$, at $\beta = 8$ (upper panels, with 13 disorder realizations in $\{t_{\alpha\beta}\}$) and $\beta = 12$ (lower panels, with 32 disorder realizations in $\{t_{\alpha\beta}\}$).

In Fig. 2 (a) and (b), we show the data at $\beta = 8$, and fit $G_b(\tau)$ and $G_f(\tau)$ according to Eq. (9), both with the power x as a free parameter and with $x = 0.098$ in the large- N solution of Eq. (4). It is interesting to see both for G_b and G_f the two fitting curves run through the data almost identically and only deviate from the numerical data close to $\tau = 0$ and $\tau = \beta$. This deviation at short times represents high-energy physics that is above the scale of interaction effects. In particular, $G_f(0, 0) = 0.5$

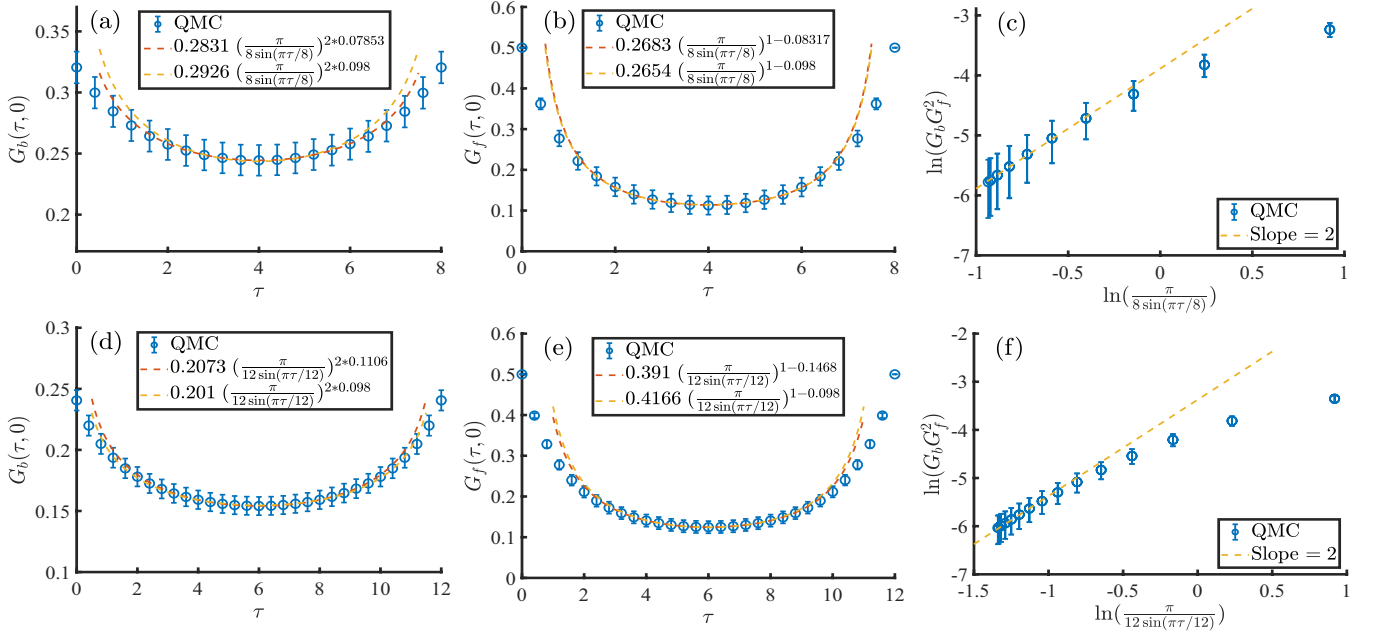


FIG. 2. DQMC results are $M = N = 6$, $m_0 = \omega_0 = 1$, $\beta = 8$ (upper panels) and $\beta = 12$ (lower panels). (a) Green's function of bosons $G_b(\tau, 0)$ versus τ in the range of $\tau \in [0, \beta]$. Blue dots are DQMC data from disorder average of 13 disorder realizations. Yellow dashed line is the fitting according to Eq. (9), with the obtained $x_b = 0.079$. Red dashed line is plotted with $x = 0.098$ – the solution of Eq. (4) – according to Eq. (9). The two dashed lines are very close to each other. (b) Green's function of fermions $G_f(\tau, 0)$ versus τ in the range of $\tau \in [0, \beta]$. Blue dots are DQMC data and the two dashed lines are the same as those in panel (a), the fitting $x_f = 0.083$ is close to the large- N result. (c) To verify the relation Eq. (10) of the nFL boson and fermion Green's functions, which means $\ln(G_b G_f^2) \propto 2 \ln\left(\frac{\pi}{\beta \sin(\pi\tau/\beta)}\right)$, we depict the $G_b G_f^2$ versus $\frac{\pi}{\beta \sin(\pi\tau/\beta)}$ in a log-log plot. The straight line with slope 2 is clearly visible. (d), (e) and (f) are the corresponding analyses at lower temperature of $\beta = 12$ and average of 32 disorder realizations to further reduce the finite temperature fluctuations, the fitting in both the Green's function of boson [(d)] and fermion [(e)] and the product of $G_b G_f^2$ [(f)] are with even smaller errorbars, suggesting that the system here has successfully entered into the nFL regime with self-tuned quantum criticality even through the parameter set $M = N = 6$ are well finite and the temperature at $\beta = 12$ is still moderately high.

is the fermion density and is fixed in our simulation at half-filling, such that the QMC data at $\tau = 0$ will not follow the expression in Eq. (9).

In comparison with the analytical result for $x = 0.098$ from Eq. (4), our fitting shows

$$G_f(\tau, 0) \propto \left(\frac{\pi}{\beta \sin(\pi\tau/\beta)}\right)^{1-x_f}, \quad x_f = 0.083$$

$$G_b(\tau, 0) \propto \left(\frac{\pi}{\beta \sin(\pi\tau/\beta)}\right)^{2x_b}, \quad x_b = 0.079. \quad (33)$$

In Fig. 2 (c), we show the product of $G_b G_f^2$ versus $\frac{\pi}{\beta \sin(\pi\tau/\beta)}$. In a log-log plot, it is clear that although the error bars in the data are still large, due to the fact that $\beta = 8$ is still a moderately high temperature and probably insufficient number of disorder averages, the slope of the $G_b G_f^2$ does approach 2 as $\tau \rightarrow \beta/2$ to the left end of the plot. Thus we see that even at moderate values of $N = M = 6$, the quantum critical and nFL behaviors consistent with large- N results can already be observed from the power-law decay of the Green's functions.

We further reduce the temperature to $\beta = 12$. The

results are shown in Fig. 2 (d), (e) and (f) in the same manner. We fit the $G_b(\tau)$ in Fig. 2 (d) and $G_f(\tau)$ in Fig. 2 (e) according to Eq. (9), both with the power x as a free parameter and with $x = 0.098$ in the large- N solution of Eq. (4). Now the fitted x values are

$$x_b = 0.111 \quad \text{and} \quad x_f = 0.147. \quad (34)$$

both reasonably close to the large- N value of $x = 0.098$, meaning that the system is indeed at the nFL with quantum critical bosons, even though in the Hamiltonian Eq. (1) the bosons have a bare mass term. In Fig. 2 (f), we plot the product of $G_b G_f^2$ versus $\frac{\pi}{\beta \sin(\pi\tau/\beta)}$ at $\beta = 12$. Now that the errorbars are smaller, due to more disorder averages and lower temperature, it is clear that the slope of the $G_b G_f^2$ approaches 2 as $\tau \rightarrow \beta/2$, consistent with the analytical results at large- N .

As discussed in Sec. II A, the self-tuned quantum criticality shall occur independent of the bare boson mass m_0 , at least at the large- N limit. We numerically tested this possibility in our QMC simulation with $M = N = 6$. The results are shown in Fig. 3. As a comparison with our interacting model, Fig. 3 (a) shows the bare boson

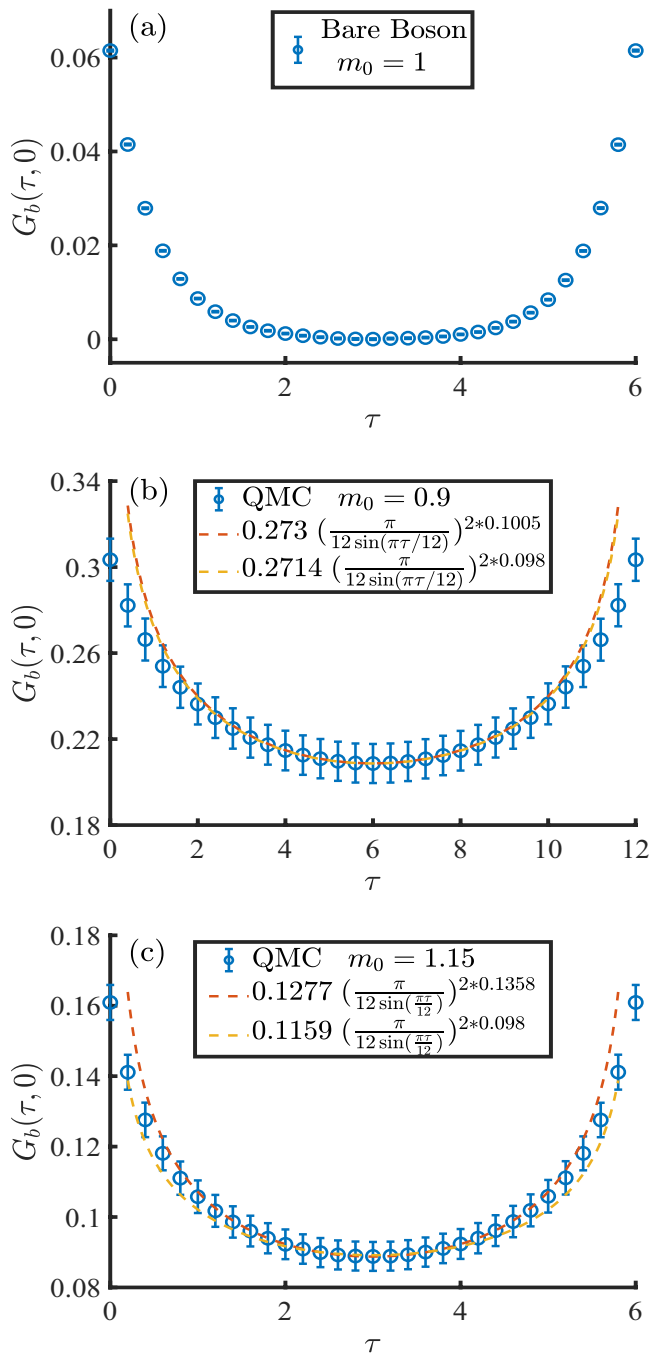


FIG. 3. Self-tuned quantum criticality with different boson masses. (a) Bare H_b without coupled to fermions, with $m_0 = 1$ and $\beta = 12$. The exponential decay in imaginary time is self-evident with $G_b(\tau = \beta/2) \sim 0$. (b) and (c) Boson Green's functions with different mass $m_0 = 0.9\omega_0$ [(b)] and $m_0 = 1.15\omega_0$ [(c)] with $\omega_0 = 1$ at $\beta = 12$. Blue dots are DQMC data and the two dashed lines are fitting similar to those in Fig. 2 where one of them are power-law function in Eq. (9) with $x = 0.098$ and the other are fitting with x as free parameter. The two lines are very close to each other and the fitting power x are close to the expected one. These results reveal the self-tuned quantum criticality in our system at $M = N = 6$ and $\beta = 12$.

Green's function generated from H_b in Eq. (18) and the mass is $m_0 = 1$ and $\beta = 12$. With such a mass term, the Green's function clearly exhibits exponential decay in imaginary time to $G_b(\tau = \beta/2, 0) \approx 0$. However, once coupled with fermions in our model, as shown in Fig. 3 (b) [$m_0 = 0.9\omega_0$, average over 18 realizations] and (c) [$m_0 = 1.15\omega_0$, average over 27 realizations], with difference masses while keeping the $M = N = 6$ and $\beta = 12$, the boson Green's functions become critical. The Green's functions G_b in imaginary time in both cases do not decay exponentially, but instead are well fitted with the power-law form of Eq. (9). In (b) and (c), besides the QMC data, we plotted two dashed lines with one of them using the expected power of $x = 0.098$ and the other fit the power x as a free parameter. The two curves turn out to be very close to each other with the fitting power close to the expected value. Remarkably, here we see that it does not require tuning the bare mass m_0 for the system to exhibit quantum-critical behavior, consistent with analytical predictions at large- N .

B. Fluctuating unconventional pairing at low temperatures

As described in Sec. II B, analytical mean-field results at $N, M \rightarrow \infty$ predicts the onset temperature T_c to be of the order of ω_0 , below which the fermionic Green's function G_f becomes gapped by the superconducting order parameter. In the time domain, $G_f(\tau)$ would decay exponentially. However, such analytical mean-field results neglects fluctuation effects of the pairing field. In particular, at any finite N, M a true pairing phase is unstable. Nevertheless, when pairing fluctuations are strong, their effects can be observed as a suppression of G_f . Here we tested the pairing behavior of our model at low temperatures.

Within our numerical capabilities, at $N = M = 6$ we were not able to go to lower temperatures than $T \equiv 1/\beta = \omega_0/12$ due to stability issues of the numerics. As we showed previously, the good agreement of our numerical data with the normal state nFL predictions indicates that the pairing gap has not developed at that temperature, in contrast with the mean-field results.

At $N = 2, M = 2$ we were able to numerically simulate the model at much lower temperatures. We show our results in Fig. 4. The upper panels of Fig. 4 depict the fermion Green's function data at $\beta = 40$ ($T = \omega_0/40$), in Fig. 4 (a) one sees the fermionic Green's function gets strongly suppressed with $G_f(\tau = \beta/2)$ close to zero. And in Fig. 4 (b) we show that the $G_f(\tau)$ can be nicely fitted by an exponential decay in imaginary time. If one fits G_f by the power-law form $\sim [1/\beta \sin(\pi\tau/\beta)]^{1-x}$, as shown in Fig. 4 (c), one would get $x = -0.506$, indicating the fermionic self-energy $\Sigma(\Omega) \propto |\omega|^x \text{sgn}(\omega)$ actually increases as frequency lowers, much different from a nFL. This shows that fluctuating pairing order has become strong to spoil the nFL behavior. In contrast, at a

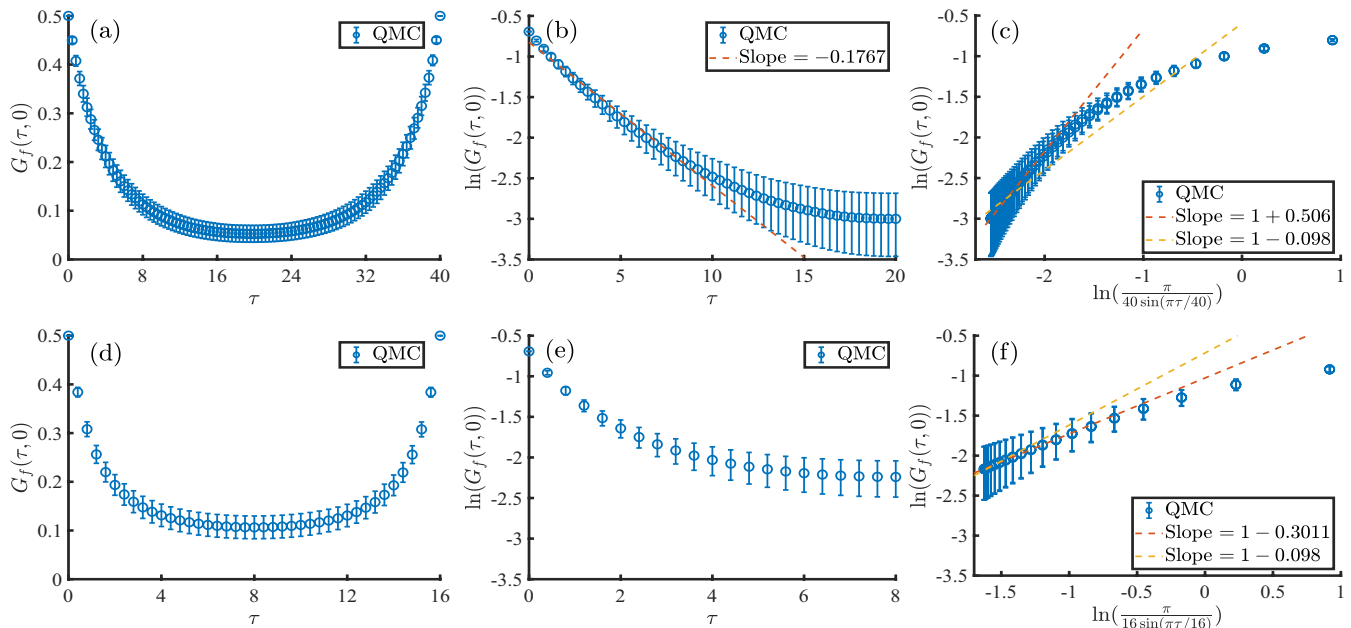


FIG. 4. Crossover from unconventional pairing to nFL at $M = N = 2$ and different temperatures. (a), (b) and (c), the fermion Green’s function at lower temperature $\beta = 40$ and $m_0 = \omega_0 = 1$, average over 12 disorder realizations. The $G_f(\tau)$ clearly demonstrates exponential decay and $G_f(\tau = \beta/2) \sim 0$ in (a). In semi-log plot in (b), the exponential decay in imaginary time can be fitted with a straight line as indicated by the yellow dashed line. And in (c), if one wants to fit $\ln(G_f)$ versus $\ln(\frac{\pi}{\beta \sin(\frac{\pi\tau}{\beta})})$ like Eq. (9): $\ln(G_f) \propto (1-x) \ln(\frac{\pi}{\beta \sin(\frac{\pi\tau}{\beta})})$, the fitting gives rise to an unphysical power $x = -0.506$, as shown by the red dashed line, much different from the nFL behavior in the yellow dashed line with $x = 0.098$. (d), (e) and (f), the fermion Green’s function at higher temperature of $\beta = 16$ and $m_0 = \omega_0 = 1$, averaged over 16 disordered realizations. In (d), the $G_f(\tau)$ decays to a finite constant value at $\tau = \beta/2$. And a semi-log plot in (e) reveals that the data do not exhibit exponential decay but rather in a power-law manner as expected for nFL as those in Fig. 2 (b) and (e). If one fit the data in $\ln(G_f)$ versus $\ln(\frac{\pi}{\beta \sin(\frac{\pi\tau}{\beta})})$ in (f), the power-law behavior in Eq. (9) can be seen with reasonable slope of 0.3 comparable with the large- N expectation of slope 0.098.

higher temperature $\beta = 16$, as shown in the lower panels (d), (e) and (f) of Fig. 4, $G_f(\tau)$ can be nicely fitted by a power law form with $x = 0.30$, indicative of a nFL behavior.

V. DISCUSSION

In this paper we have performed unbiased sign-problem-free quantum Monte Carlo simulations of the Yukawa-SYK model, and reported direct evidence of self-tuned quantum-critical and nFL behaviors. We have also shown evidence of strong pairing fluctuations from a nFL high-temperature “parent state”. SYK-like models have provided a new venue to construct analytical solvable models for strange metals and unconventional superconductors. Our work serves as a starting point of further analyzing such models beyond the analytical large- N limit, in a numerically unbiased manner. Several further directions are in order.

First, it would be interesting to construct a lattice version of the Yukawa-SYK model. Several analytical attempts [52–54] have been put forward by coupling a

large number of SYK models. However, such a realization is numerically difficult to realize due to the fermion sign problem and the introduction of an additional degree of freedom. Within our model, on the other hand, one can treat the α, β degree of freedom as lattice sites and add lattice hopping terms between them, as a natural extension of the current model. It is an open analytical and numerical problem to study such a lattice model, including its spectral and transport properties. Second, in the present quantum-dot model, the large fluctuation effects strongly suppress the pairing instability, and we observed signatures of pairing only at very low temperatures. In a lattice extension of the current model, we expect the signatures of superconductivity to be much more robust. Our model therefore serves as an ideal and numerically concrete platform to systematically study the pairing problem for non-Fermi liquids in the future, shedding light on the nature of unconventional superconductors.

ACKNOWLEDGEMENT

We thank Subir Sachdev, Steven Kivelson for insightful discussions. G.P.P thanks Rui-Zhen Huang for helpful discussion on numerical calculations. We acknowledge the supports from the Ministry of Science and Technology of China through the National Key Research and Development Program (Grant No. 2016YFA0300502), the National Science Foundation of China (Grant Nos. 11574359,11674370) and Research Grants Council of Hong Kong Special Administrative Region of China through 17303019. We thank the Center for Quantum Simulation Sciences in the Institute of Physics, Chinese Academy of Sciences, the Computational Initiative at the Faculty of Science at the University of Hong Kong and the Tianhe-1A platform at the National Supercomputer Center in Tianjin and Tianhe-2 platform at the National Supercomputer Center in Guangzhou for their technical support and generous allocation of CPU time. This research was initiated at the Aspen Center for Physics, supported by NSF PHY-1066293.

Appendix A: Monte Carlo measurements

The ensemble average of physical observables, in the DQMC formalism, can be calculated as,

$$\begin{aligned}
\langle \hat{O} \rangle_C &= \frac{\partial}{\partial \eta} \ln \text{Tr} \left[\hat{U}_C(\beta, \tau) e^{\eta \hat{O}} \hat{U}_C(\tau, 0) \right] \Big|_{\eta=0} \\
&= \frac{\partial}{\partial \eta} \ln \text{Det} \left[\mathbf{1} + B_C(\beta, \tau) e^{\eta O} B_C(\tau, 0) \right] \Big|_{\eta=0} \\
&= \frac{\partial}{\partial \eta} \text{Tr} \ln \left[\mathbf{1} + B_C(\beta, \tau) e^{\eta O} B_C(\tau, 0) \right] \Big|_{\eta=0} \\
&= \text{Tr} \left[B_C(\tau, 0) (1 + B_C(\beta, 0))^{-1} B_C(\beta, \tau) O \right] \\
&= \text{Tr} \left[(1 - (1 + B_C(\tau, 0) B_C(\beta, \tau))^{-1}) O \right] \quad (\text{A1})
\end{aligned}$$

in the case of equal time fermionic Green's function, $\hat{O} = \hat{c}^\dagger O \hat{c}$. \hat{U}_C and B_C are defined in Eq. (23) and Eq. (32) in the main text, respectively.

For the imaginary time displaced fermionic Green's function, $G_{f,ij}(\tau, 0) = \langle c_i(\tau) c_j^\dagger(0) \rangle$ where i, j encapsulate the dot, flavor and spin indices in the Hamiltonian in Eq. (1) and the imaginary time $\tau \in [0, \beta]$, it can be evaluated in DQMC as

$$\begin{aligned}
\langle c_i(\tau) c_j^\dagger(0) \rangle &= \frac{\text{Tr} \{ \hat{U}_C(\beta, \tau) \hat{c}_i \hat{U}_C(\tau, 0) \hat{c}_j^\dagger \}}{\text{Tr} \{ \hat{U}_C(\beta, 0) \}} \\
&= \frac{\text{Tr} \{ \hat{U}_C(\beta, 0) \left[\hat{U}_C^{-1}(\tau, 0) \hat{c}_i \hat{U}_C(\tau, 0) \right] \hat{c}_j^\dagger \}}{\text{Tr} \{ \hat{U}_C(\beta, 0) \}} \\
&= \sum_k B_C(\tau, 0)_{ik} \frac{\text{Tr} \{ \hat{U}_C(\beta, 0) \hat{c}_k \hat{c}_j^\dagger \}}{\text{Tr} \{ \hat{U}_C(\beta, 0) \}} \\
&= [B_C(\tau, 0) (1 + B_C(\beta, 0))^{-1}]_{ij} \quad (\text{A2})
\end{aligned}$$

where the intermediate steps in Eq. (A2) are given explicitly in Ref. [42].

-
- [1] G. R. Stewart, *Rev. Mod. Phys.* **73**, 797 (2001).
[2] A. Abanov, A. Chubukov, and J. Schmalian, *Advances in Physics* **52**, 119 (2003).
[3] B. Keimer, S. A. Kivelson, M. R. Norman, S. Uchida, and J. Zaanen, *Nature* **518**, 179 (2015).
[4] Z. Liu, Y. Gu, W. Zhang, D. Gong, W. Zhang, T. Xie, X. Lu, X. Ma, X. Zhang, R. Zhang, J. Zhu, C. Ren, L. Shan, X. Qiu, P. Dai, Y.-f. Yang, H. Luo, and S. Li, *Phys. Rev. Lett.* **117**, 157002 (2016).
[5] Y. Gu, Z. Liu, T. Xie, W. Zhang, D. Gong, D. Hu, X. Ma, C. Li, L. Zhao, L. Lin, Z. Xu, G. Tan, G. Chen, Z. Y. Meng, Y.-f. Yang, H. Luo, and S. Li, *Phys. Rev. Lett.* **119**, 157001 (2017).
[6] J. Custers, P. Gegenwart, H. Wilhelm, K. Neumaier, Y. Tokiwa, O. Trovarelli, C. Geibel, F. Steglich, C. Pálpin, and P. Coleman, *Nature* **424**, 524 (2003).
[7] B. Shen, Y. Zhang, Y. Komijani, M. Nicklas, R. Borth, A. Wang, Y. Chen, Z. Nie, R. Li, X. Lu, H. Lee, M. Smidman, F. Steglich, P. Coleman, and H. Yuan, arXiv e-prints, arXiv:1907.10470 (2019), arXiv:1907.10470 [cond-mat.str-el].
[8] Y. Cao, D. Chowdhury, D. Rodan-Legrain, O. Rubies-Bigordà, K. Watanabe, T. Taniguchi, T. Senthil, and P. Jarillo-Herrero, arXiv e-prints, arXiv:1901.03710 (2019), arXiv:1901.03710 [cond-mat.str-el].
[9] S. Sachdev and J. Ye, *Phys. Rev. Lett.* **70**, 3339 (2015).
[10] A. Kitaev, *Entanglement in Strongly-Correlated Quantum Matter*.
[11] S. Sachdev, *Phys. Rev. X* **5**, 041025 (2015).
[12] A. Kitaev and S. J. Suh, *Journal of High Energy Physics* **2018**, 183 (2018).
[13] Y. Gu, X.-L. Qi, and D. Stanford, *Journal of High Energy Physics* **2017**, 125 (2017).
[14] M. A. Metlitski and S. Sachdev, *Phys. Rev. B* **82**, 075127 (2010).

- [15] M. A. Metlitski and S. Sachdev, Phys. Rev. B **82**, 075128 (2010).
- [16] M. A. Metlitski, D. F. Mross, S. Sachdev, and T. Senthil, Phys. Rev. B **91**, 115111 (2015).
- [17] S. Raghu, G. Torroba, and H. Wang, Phys. Rev. B **92**, 205104 (2015).
- [18] S. Lederer, Y. Schattner, E. Berg, and S. A. Kivelson, Phys. Rev. Lett. **114**, 097001 (2015).
- [19] M. J. Lawler, D. G. Barci, V. Fernández, E. Fradkin, and L. Oxman, Phys. Rev. B **73**, 085101 (2006).
- [20] M. J. Lawler and E. Fradkin, Phys. Rev. B **75**, 033304 (2007).
- [21] X. Y. Xu, K. Sun, Y. Schattner, E. Berg, and Z. Y. Meng, Phys. Rev. X **7**, 031058 (2017).
- [22] Z. H. Liu, X. Y. Xu, Y. Qi, K. Sun, and Z. Y. Meng, Phys. Rev. B **98**, 045116 (2018).
- [23] Z. H. Liu, G. Pan, X. Y. Xu, K. Sun, and Z. Y. Meng, Proceedings of the National Academy of Sciences **116**, 16760 (2019).
- [24] X. Y. Xu, Y. Qi, L. Zhang, F. F. Assaad, C. Xu, and Z. Y. Meng, Phys. Rev. X **9**, 021022 (2019).
- [25] X. Y. Xu, Z. H. Liu, G. Pan, Y. Qi, K. Sun, and Z. Y. Meng, Journal of Physics: Condensed Matter **31**, 463001 (2019).
- [26] S.-S. Lee, Phys. Rev. B **80**, 165102 (2009).
- [27] E. Berg, M. Metlitski, and S. Sachdev, Science **338**, 1606 (2012).
- [28] E. Berg, S. Lederer, Y. Schattner, and S. Trebst, Annual Review of Condensed Matter Physics **10**, 63 (2019).
- [29] Y. Schattner, S. Lederer, S. A. Kivelson, and E. Berg, Phys. Rev. X **6**, 031028 (2016).
- [30] M. H. Gerlach, Y. Schattner, E. Berg, and S. Trebst, Phys. Rev. B **95**, 035124 (2017).
- [31] X. Wang, Y. Schattner, E. Berg, and R. M. Fernandes, Phys. Rev. B **95**, 174520 (2017).
- [32] C. Bauer, Y. Schattner, S. Trebst, and E. Berg, arXiv e-prints, arXiv:2001.00586 (2020), arXiv:2001.00586 [cond-mat.str-el].
- [33] C. Chen, X. Y. Xu, Y. Qi, and Z. Y. Meng, arXiv e-prints, arXiv:1904.12872 (2019), arXiv:1904.12872 [cond-mat.str-el].
- [34] A. Klein and A. Chubukov, Phys. Rev. B **96**, 041125 (2017).
- [35] Y. Wang, arXiv e-prints, arXiv:1904.07240 (2019), arXiv:1904.07240 [cond-mat.str-el].
- [36] I. Esterlis and J. Schmalian, Phys. Rev. B **100**, 115132 (2019).
- [37] D. Hauck, M. J. Klug, I. Esterlis, and J. Schmalian, arXiv e-prints, arXiv:1911.04328 (2019), arXiv:1911.04328 [cond-mat.str-el].
- [38] J. Kim, X. Cao, and E. Altman, arXiv e-prints, arXiv:1910.10173 (2019), arXiv:1910.10173 [cond-mat.str-el].
- [39] The Fourier transform from $\Pi(\Omega)$ is tricky, since the positive power-law $|\Omega|^{1-2x}$ does not have a Fourier transform in the common sense as the Fourier integral is UV divergent for $0 < x < 1/2$. This divergence is canceled by the Fourier transform of the m_0^2 term in $\Pi(\Omega)$ with the UV information.
- [40] R. Blankenbecler, D. J. Scalapino, and R. L. Sugar, Phys. Rev. D **24**, 2278 (1981).
- [41] J. E. Hirsch, Physical Review B **28**, 4059 (1983).
- [42] J. E. Hirsch, Phys. Rev. B **31**, 4403 (1985).
- [43] F. Assaad and H. Evertz, in *Computational Many-Particle Physics*, Lecture Notes in Physics, Vol. 739, edited by H. Fehske, R. Schneider, and A. Weiße (Springer Berlin Heidelberg, 2008) pp. 277–356.
- [44] M. Brunner, F. F. Assaad, and A. Muramatsu, Phys. Rev. B **62**, 15480 (2000).
- [45] F. F. Assaad, Phys. Rev. Lett. **83**, 796 (1999).
- [46] M. Hohenadler, Z. Y. Meng, T. C. Lang, S. Wessel, A. Muramatsu, and F. F. Assaad, Phys. Rev. B **85**, 115132 (2012).
- [47] Z. Y. MENG, H.-H. HUNG, and T. C. LANG, Modern Physics Letters B **28**, 1430001 (2014), <https://doi.org/10.1142/S0217984914300014>.
- [48] Y.-Y. He, H.-Q. Wu, Y.-Z. You, C. Xu, Z. Y. Meng, and Z.-Y. Lu, Phys. Rev. B **93**, 115150 (2016).
- [49] Y. Q. Qin, Y.-Y. He, Y.-Z. You, Z.-Y. Lu, A. Sen, A. W. Sandvik, C. Xu, and Z. Y. Meng, Phys. Rev. X **7**, 031052 (2017).
- [50] Y. Liu, W. Wang, K. Sun, and Z. Y. Meng, arXiv e-prints, arXiv:1910.07430 (2019), arXiv:1910.07430 [cond-mat.stat-mech].
- [51] C. Wu and S.-C. Zhang, Phys. Rev. B **71**, 155115 (2005).
- [52] X.-Y. Song, C.-M. Jian, and L. Balents, Phys. Rev. Lett. **119**, 216601 (2017).
- [53] Z. Bi, C.-M. Jian, Y.-Z. You, K. A. Pawlak, and C. Xu, Phys. Rev. B **95**, 205105 (2017).
- [54] D. Chowdhury, Y. Werman, E. Berg, and T. Senthil, Phys. Rev. X **8**, 031024 (2018).